Pol. J. Environ. Stud. Vol. 33, No. 2 (2024), 1455-1465
DOI: *10.15244/pjoes/173168* ONLINE PUBLICATION DATE: 2023-12-04

Original Research

Mild Acid-Alkali Modification of Ceramsite: a Low-Cost Adsorbent for Lead Removal

Xingbo Yuan[1], Ziqiu Wang[1], Chuan Wang[1, 2]*

[1]School of Ecology & Environment, Inner Mongolia University, Hohhot 010021, China
[2]Inner Mongolia Key Laboratory of Environmental Pollution Control & Waste Resource Reuse, Inner Mongolia University, Hohhot 010021, China

Received: 29 June 2023
Accepted: 2 October 2023

Abstract

In order to improve the adsorption capacity of waste-based ceramsite, this study proposed to use acid-alkali surface modification to enhance the adsorption capacity of ceramsite for heavy metals. In acid treatment, the ceramsite surface generated a composite pore structure, thus the specific surface area of ceramsite is significantly increased through acid treatment. In alkaline treatment, hydroxyl functional groups were loaded on the surface of the ceramsite, therefore the adsorption capacity for heavy metals was significantly improved. The surface of modified ceramic particles carries a negative charge, which is beneficial for the adsorption of cations. Taking lead ions as an example, the adsorption performance of ceramic particles on heavy metals was tested, and the maximum adsorption capacity reached 33.2 mg/g. Furthermore, the modified ceramic particles exhibit good desorption and regeneration properties. The modified ceramsite offers advantages in terms of raw material sources and production costs compared to natural zeolite.

Keywords: ceramsite, surface modification, specific surface area, heavy metals, adsorption capacity

Introduction

Ceramsite are currently widely used as artificial water treatment filter media, since ceramsite have the characteristics of porosity, biocompatibility, and high strength, making them suitable as microbial carriers in the domestic wastewater treatment process [1-6]. Although sintered ceramsite have a macroscopic large pore structure but a relatively smooth microscopic surface, so there are almost no microporous and mesoporous structures on the surface of ceramsite [7, 8]. Therefore, the specific surface area of the original sintered ceramsite is relatively small, resulting in poor adsorption capacity, far lower than that of other filter medias such as zeolite and activated carbon [9-11].

In order to enhance the role of ceramsite in wastewater treatment, researchers have attempted to generate micro-porous structures on the surface of ceramsite to increase its specific surface area, adsorption capacity and loading capacity [11-17]. The study by Chuan et al. [7, 18]. shows that the chemical activity of the internal phase of ceramsite have been increased during the high-temperature sintering process. Moreover, it was found that under alkaline hydrothermal conditions, the silicon and aluminum components inside ceramsite can be transformed into zeolite structures,

*e-mail: wangchuan437@126.com

thereby forming hierarchical pore structures on the surface and increasing its specific surface area and adsorption capacity. In subsequent studies, Zhang et al. [8, 19] analyzed the mechanism of zeolite crystallization on the surface of ceramsite. Furthermore, researchers have applied surface-zeolitized ceramsite in the removal of heavy metals or ammonia nitrogen from aqueous solutions, and the zeolitized modification by the alkaline hydrothermal process significantly increased the specific surface area and adsorption capacity of ceramsite, resulting in good removal effects [7, 8, 18-20]. However, the alkaline hydrothermal modification process requires a lengthy reaction time (typically exceeding 6 hours) and harsh reaction conditions (high temperature and high pressure). This result in high costs and low operability when applying the alkaline hydrothermal modification technology for ceramsite.

To address the issue of high costs and low operability of ceramsite hydrothermal modification mentioned above, the purpose of this study is to develop a new surface modification technology for ceramsite, which should be mild in reaction conditions and easy to implement. Based on the chemical composition and surface characteristics of ceramsite, a novel acid-alkali combined modification method is proposed for the first time.

In recent years, extensive literature has reported the use of substances such as algae, sugarcane bagasse, zeolite, etc. to prepare various low-cost adsorbent materials capable of adsorbing pollutants such as dyes or heavy metals [21-27]. Inspired by this, the present study attempts to make ceramsite an efficient environmental functional material through modification techniques. In order to test the application effectiveness of modified ceramsite with high surface area as an environmental functional material, the modified ceramsite were used in the treatment process of lead-containing wastewater in Inner Mongolia region. There are various treatment technologies for lead-containing wastewater, such as oxidation, ion exchange, precipitation, and electrochemical treatment. Considering the local conditions and treatment cost, we chose to use the modified ceramsite as a cation adsorbent to remove lead ions from water. In summary, this study provides a novel surface modification technology for ceramsite, which cound promote the deep application of ceramsite in wastewater treatment.

Material and Methods

Material

The ceramsite used in this study were prepared from four typical solid wastes in the laboratory, including construction and demolition waste (C&D), fly ash (FA), red mud (RM), and rice husk ash (RHA). The first three components mentioned (C&D, FA and RM) are the main ceramic components, while RHA is used as a pore-forming agent. The chemical compositions of the four raw materials and sintered ceramsite (SC) were determined using X-ray fluorescence spectrometry, and the results are shown in Table 1.

Ceramsite Preparation

The whole experimental procedure of this study is illustrated in Fig. 1. The composition and function of each part of the ceramsite are as follows: construction and demolition waste is the main material, fly ash is the silicon-aluminum adjuster, red mud is the flux, and rice husk ash is the pore-forming agent. The ratio of the raw materials is as follows: construction waste: fly ash: red mud: rice husk ash = 10:2:3:1.5. The sintering conditions are as follows: sintering temperature of 1150ºC and a holding time of 10 minutes. The properties of the ceramsite are as follows: bulk density of 0.663 cm^3/g, apparent density of 1.189 cm^3/g, porosity of 44.268%, and water absorption of 3.32%.

Acid Treatment of Ceramsite

First, the ceramsite are crushed into uniform particles with a size of 8-10 mm and then placed in a certain volume of sulfuric acid solution and stirred on a magnetic stirrer at a rate of 300 rpm. After the Acid treatment process is completed, solid-liquid separation is carried out by filtering, and the solid product is washed three times with deionized water using ultrasonic waves, then dried at 105ºC to obtain the acid-treated ceramsite.

Alkali Modification of Ceramsite

The acid-treated ceramsite were placed in a NaOH solution under the following reaction conditions: liquid-to-solid ratio of 10:1, magnetic stirring speed

Table 1. Chemical composition of raw materials and ceramsite (wt.%).

	SiO_2	Al_2O_3	Fe_2O_3	K_2O	Na_2O	CaO	MgO	Others
C&D	63.24	12.51	4.09	3.06	2.30	11.68	1.81	1.31
FA	42.07	36.35	7.05	0.89	0.32	6.52	0.26	6.55
RM	9.50	4.02	21.09	0.90	0.54	52.30	0.36	11.30
RHA	77.18	0.39	2.76	6.33	0.49	2.32	0.24	10.29
SC	55.33	13.31	6.05	2.24	1.98	17.41	1.08	2.60

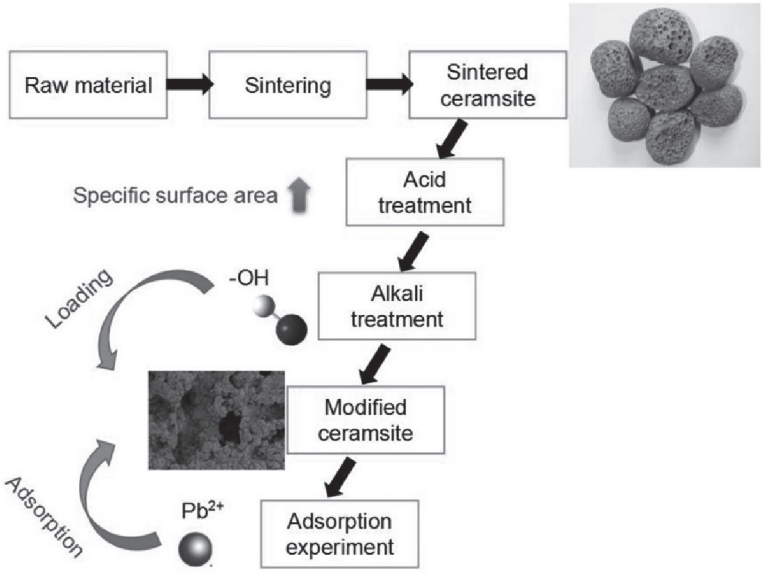

Fig. 1. Schematic diagram for the preparation and modification of ceramsite.

of 300 r/min, and reaction temperature of 60ºC. After 6 hours of alkaline treatment solid-liquid separation was performed, and the solid product was washed three times with deionized water by ultrasonic treatment, and then dried at 105ºC to obtain the Alkali modified ceramsite.

Adsorption Test

0.5 g of the adsorbent was added into a series of conical flasks containing 50 mL of lead nitrate solution with concentrations of 50, 100, 200, 300, 400, 500, 600, and 700 mg/L. The system was stirred at 300 rpm, and the pH was controlled to be less than 6 to prevent the precipitation of lead nitrate. After a 6-hour adsorption period, the concentration of Pb^{2+} in the conical flask was determined.

Adsorbent Regeneration

Spent adsorbent were obtained after adsorbing lead ions from a lead nitrate solution with a concentration of 500 mg/L. The spent ceramsite were then subjected to a desorption process in a 1 mol/L hydrochloric acid solution for 30 minutes. Then, to reload hydroxyl groups, they were immersed in a 4 mol/L sodium hydroxide solution and reacted at 60ºC for 30 minutes. The regenerated modified ceramsite were subsequently obtained after drying.

Analysis and Characterization

Observation of surface morphology was carried out using a scanning electron microscope (TESCAN MIRA4). Ion concentration in the solution was determined using inductively coupled plasma optical emission spectrometry (Agilent 5110). X-ray diffraction analysis was performed using PANalytical Axios with the following parameters: Cu target, scanning angle range of 10° to 80°, scanning step of 0.02, scanning speed of 5°/min, working voltage of 40 kV, and current of 40 mA.

Results and Discussion

Effect of Acid Treatment Conditions on Ceramsite

The effect of Acid treatment conditions on the Acid treatment of ceramsite was studied with the specific surface area as the main evaluation index. Multiple experimental results showed that the factors that significantly affect the specific surface area of acid-modified ceramsite include acid concentration (Fig. 2a), reaction temperature (Fig. 2b), and reaction time (Fig. 2c). Among these factors, reaction time and acid concentration have a noticeable threshold effect on the specific surface area, such that exceeding a certain value leads to a significant decrease in the modification effect. For instance, when the acid concentration is higher than 5 mol/L and the reaction time exceeds 4 hours, the specific surface area no longer increases significantly, as shown in Fig. 2a) and Fig. 2b). However, reaction temperature shows a significant positive correlation with the specific surface area, as demonstrated in Fig. 2c), without a clear threshold. It should be noted that when the reaction temperature exceeds 80ºC, the loss of reaction liquid due to the high temperature of the water bath intensifies. Therefore, after comprehensive consideration, the optimized Acid treatment conditions chosen in this study are a reaction temperature of 80ºC, an acid concentration of 5 mol/L, and a reaction time of 4 hours.

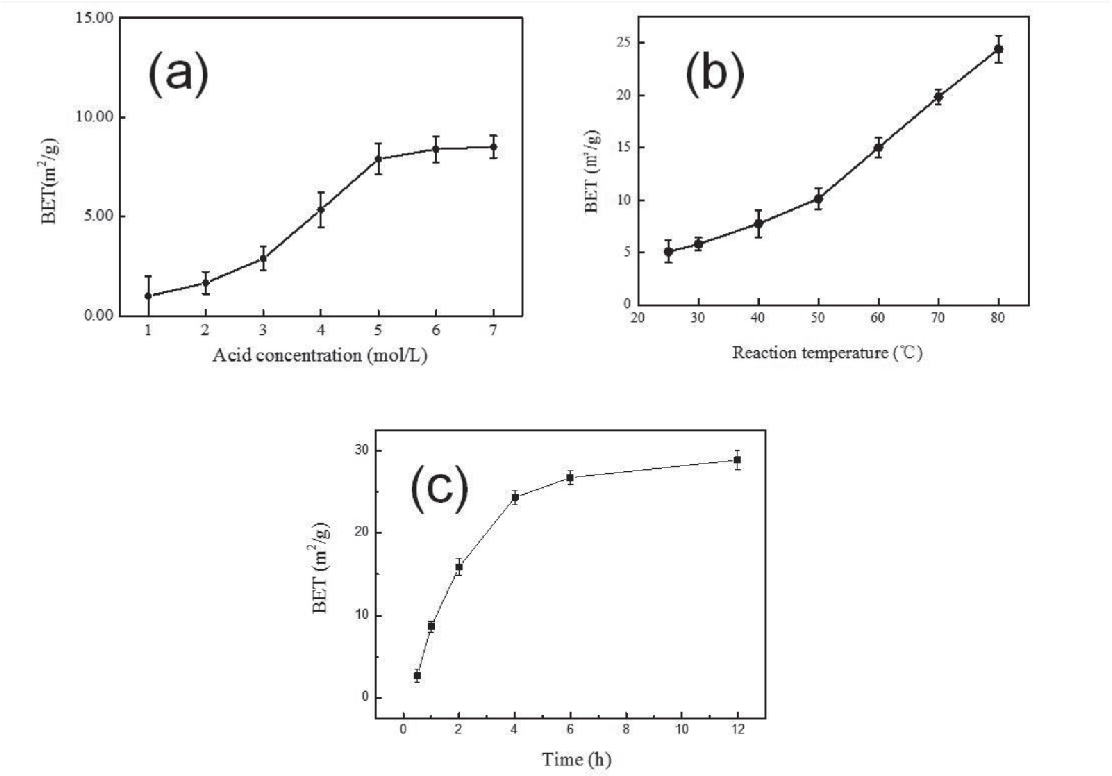

Fig. 2. Effect of reaction parameters on the specific surface area of products: a) acid concentration; b) reaction temperature; c) reaction time.

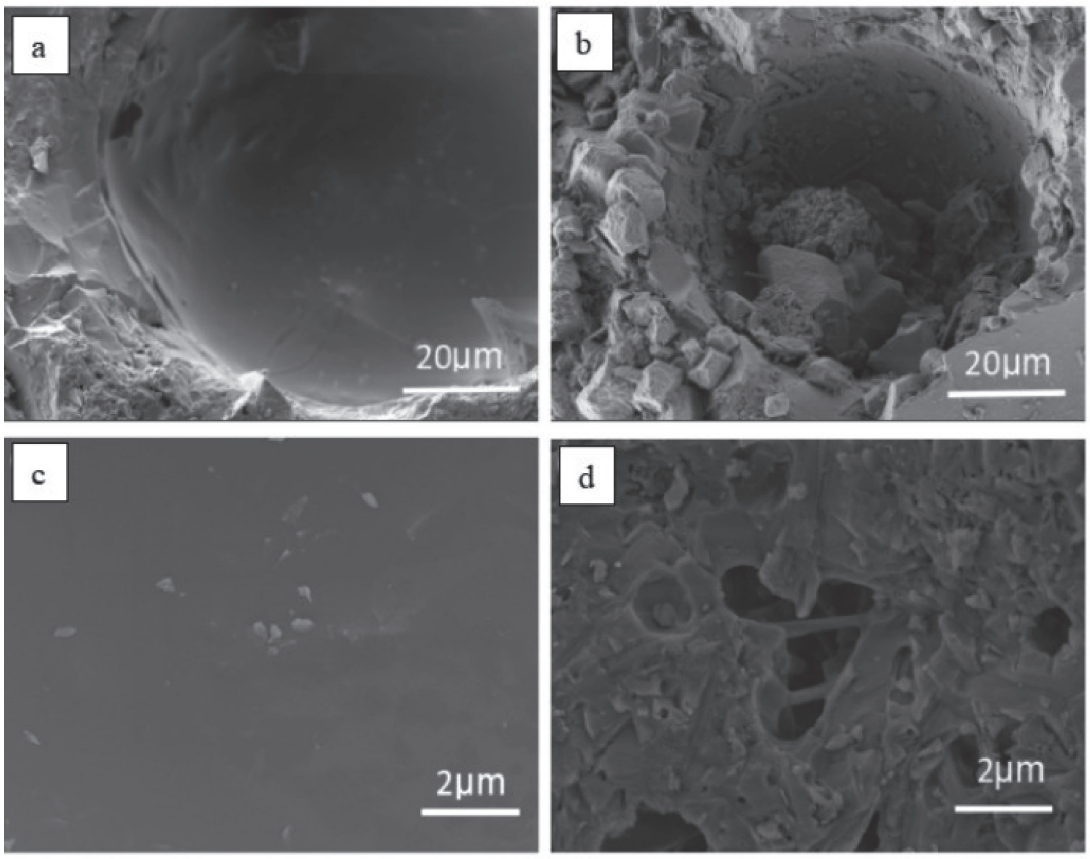

Fig. 3. SEM picture of ceramsite particles before (a, c) and after (b, d) Acid treatment.

Table 2. Chemical composition of ceramsite before and after modification (wt.%).

	SiO_2	Al_2O_3	Fe_2O_3	CaO	Na_2O	MgO
Before	55.331	13.308	6.045	17.414	1.979	1.079
After	63.185	10.503	5.074	13.567	1.629	0.744

Characterization of Acid-Treated Ceramsite

The microstructures of the ceramsite before and after Acid treatment were observed as shown in Fig. 3. The original ceramsite formed a pore structure during the sintering process due to the inclusion of some gas in the molten state, with pore sizes ranging from 100 to 800 μm. Since the sintering temperature reached 1150ºC during preparation, the ceramsite were sintered and a dense and smooth enamel structure was formed on ceramsite surface. Because the inner wall of the pores was smooth and flat, the specific surface area of the ceramsite before modification was very small, only 0.31 m^2/g. In Fig. 3b), the surface of the acid-treated modified ceramsite showed significant changes, becoming rougher and forming microstructures at a smaller scale. By further increasing the magnification, smaller pore structures with sizes of about 1-5 μm were observed on the surface of the ceramsite in Fig. 2d). Overall, the formation of new small pore structures was mainly due to the obvious etching effect on the ceramsite surface during Acid treatment, resulting in the significant increase in specific surface area of the ceramsite.

The ceramsite before and after Acid treatment were analyzed by XRF and XRD, and the results are shown in Table 2 and Fig. 4, respectively. According to Table 2, the relative content of metal elements such as calcium, aluminum, iron, sodium, and magnesium in the modified ceramsite was significantly reduced, which confirms the etching reaction of the ceramsite under Acid treatment and leads to the release of some metal ions into the solution. As shown in Fig. 4, the main phases of the acid-treated ceramsite are quartz, pyroxene, calcite, and diopside. There is no significant change in the phases after Acid treatment. Based on the above analysis, it can be concluded that (1) minerals such as diopside, calcite, and pyroxene react with acid during the Acid treatment, causing metal elements such as calcium, aluminum, and iron to detach from ceramsite surface in the form of ions and enter the solution, resulting in a general reduction in their relative content; (2) quartz has a high content and extremely stable chemical properties, which ensures that the composite pore structure of the ceramsite after Acid treatment has a basic framework.

Reaction Mechanism of Ceramsite Acid Treatment

Further analysis of the crystal structure reveals that the calcium feldspar is a framework silicate, with a crystal structure belonging to the triclinic system, while the pyroxene mineral belongs to the chain-structured silicates and the monoclinic system of the clinopyroxene subgroup. The easily soluble alkali or alkaline earth metals in the crystal cells of these

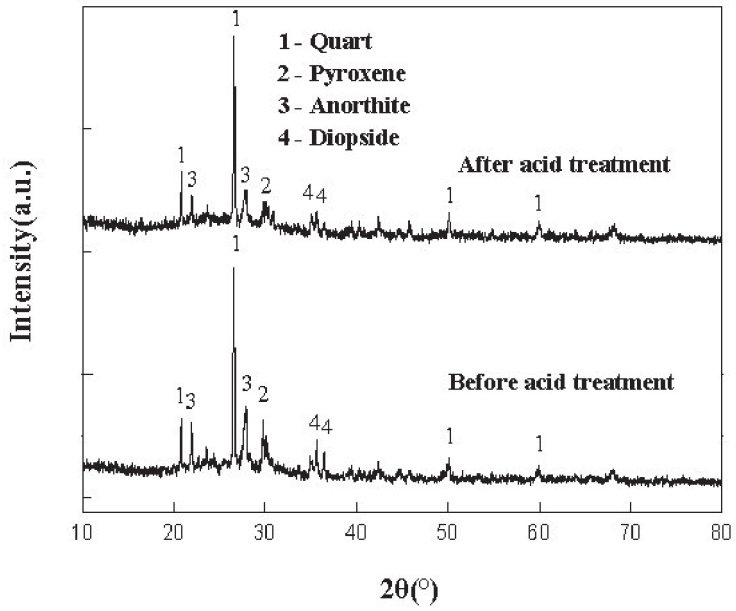

Fig. 4. Phase composition of ceramsite before and after acid treatment.

substances can react with acids. The chemical reactions of calcium feldspar and pyroxene with acid are shown in Equations (1) and (2), respectively [28-31].

$$CaO{\cdot}Al_2O_3{\cdot}2SiO_2 + H^+ \rightarrow Al_2O_3{\cdot}2SiO_2 + Ca^{2+} + H_2O \quad (1)$$

$$CaO{\cdot}MgO{\cdot}2SiO_2 + H^+ \rightarrow SiO_2 + Ca^{2+} + Mg^{2+} + H_2O \quad (2)$$

Overall, in the Acid treatment process, silicate minerals in the ceramsite undergo dissolution reactions, leading to the release of some cations such as calcium, aluminum, and iron into the solution, while the stable silicon oxide framework is preserved. Under the effect of dissolution, a micro-porous structure is formed on the surface of the ceramsite. The macro-porous structure formed during the sintering process and the micro-porous structure formed by dissolution together constitute the composite pore structure, resulting in a significant increase in the specific surface area of the ceramsite after Acid treatment.

Effect of Alkali Modification for Ceramsite

After Acid treatment, the ceramsite formed a composite pore structure and had the potential as an adsorbent material. However, experimental tests showed that acid-treated ceramsite had poor adsorption efficiency for typical heavy metal Pb^{2+} ions (adsorption capacity was only 7.9 mg/g). Therefore, this study used an alkaline treatment method to introduce hydroxyl functional groups onto the surface of the ceramsite, in order to enhance their adsorption capacity for Pb^{2+}. The infrared spectroscopy characterization results of the ceramsite before and after alkaline treatment are shown in Fig. 5, which indicates that the modified ceramic samples obtained after alkaline treatment exhibited obvious hydroxyl functional group peaks at 3456 cm^{-1}, indicating that hydroxyl groups have been loaded onto the surface of the ceramsite.

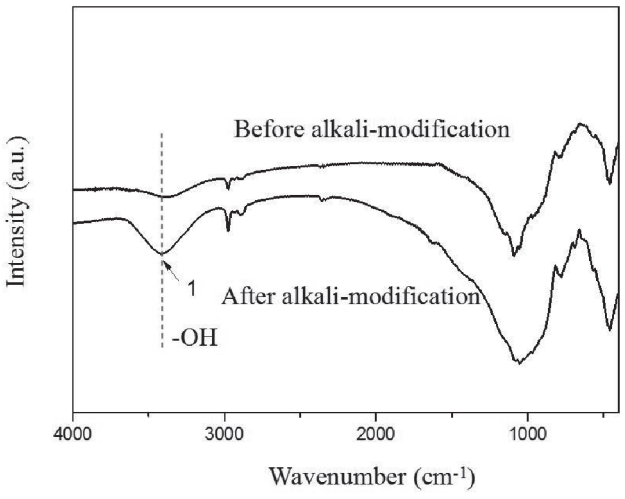

Fig. 5. Infrared spectrogram of ceramsite before and after alkali treatment.

Adsorption Capacity of Modified Ceramsite for Pb^{2+}

To investigate the kinetics of the adsorption process, the pseudo-first-order, pseudo-second-order, and Elovich kinetic models were used to fit the experimental adsorption data [32-42]. The three kinetic models equation used in this study is as follows respectively:
Pseudo-first-order:

$$\ln(q_e - q_t) = \ln q_e - k_1 t \quad (3)$$

Pseudo-second-order:

$$\frac{t}{q_t} = \frac{1}{k_2 q_e^{\,2}} + \frac{t}{q_e} \quad (4)$$

Elovich:

$$q_t = \frac{\ln(\alpha\beta)}{\beta} + \frac{\ln t}{\beta} \quad (5)$$

where k_1 represents the rate constant of the pseudo-first-order kinetic model, t is the sampling time in minutes, k_2 is the rate constant of the pseudo-second-order kinetic model, qe is the equilibrium adsorption capacity in mg/g, and qt is the adsorption capacity of the adsorbent for arsenate at time t in mg/g.

The fitting results of adsorption kinetics are presented in Fig. 6 and Table 3. Among the three adsorption kinetic models, the pseudo-second-order model exhibited the best fitting performance, with a correlation coefficient of 0.998.

The removal capacity of modified ceramsite for Pb^{2+} was evaluated using isothermal adsorption experiments, and the adsorption isotherm was fitted using the Langmuir model and Freundlich model. The two isotherm equation used in this study is as follows respectively:

$$\frac{C_e}{q_e} = \frac{1}{q_{max}} C_e + \frac{1}{K_L q_{max}} \quad (6)$$

where q_e is the equilibrium adsorption capacity (mg/g); C_e is the equilibrium concentration of Pb^{2+} (mg/L); q_{max} is the maximum adsorption capacity (mg/g); and K_L is the Langmuir adsorption constant.

$$\ln q_e = \ln K_F + \frac{1}{n} \ln C_e \quad (7)$$

where q_e is the equilibrium adsorption capacity (mg/g); C_e is the equilibrium concentration of Pb^{2+} (mg/L); n

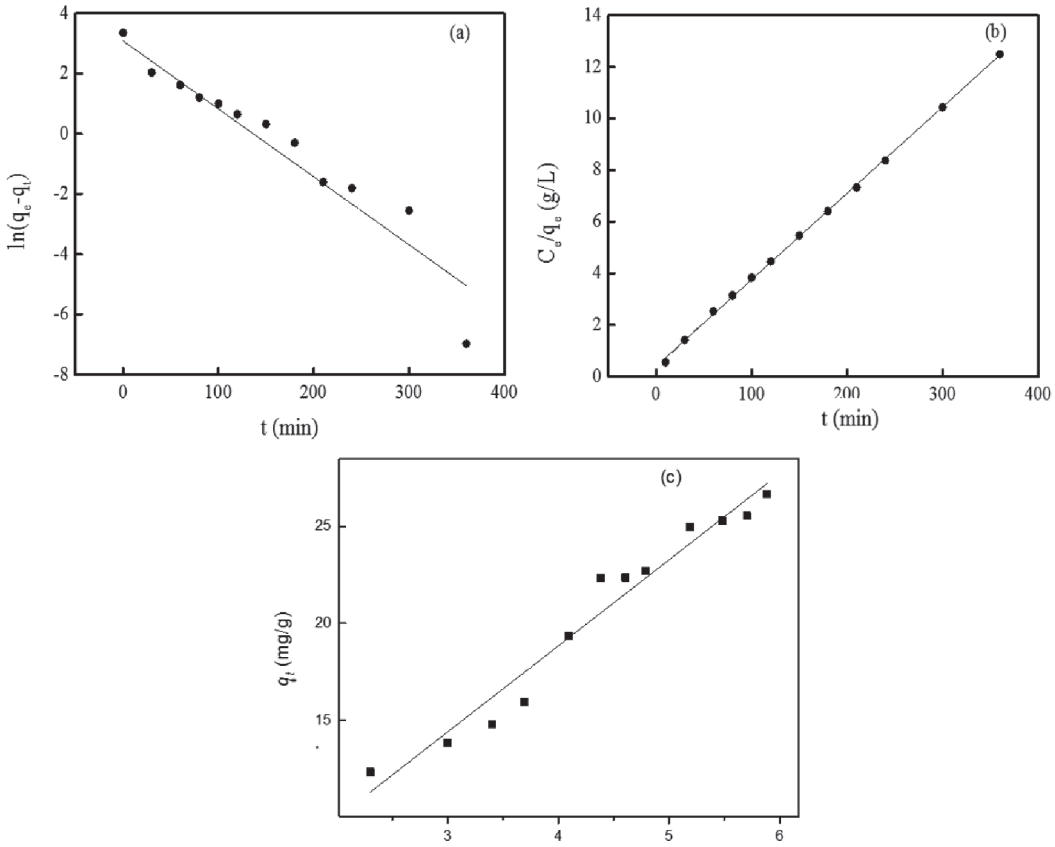

Fig. 6. Kinetic models and fitting results: a) Pseudo-first-order model; b) Pseudo-second-order model; c) Elovich model.

Table 3. Parameters and error functions for kinetic models.

	Parameters	SSE	MSE	RMSE	R^2
Pseudo-first-order	$k_1 = 0.022$	6.95	0.463	0.681	0.92
Pseudo-second-order	$k_2 = 27.027$	0.125	0.009	0.094	0.998
Elovich	$\alpha = 5.733$, $\beta = 0.226$	11.27	0.939	0.969	0.956

is a constant related to the adsorption capacity; K_F is the Freundlich equilibrium constant.

The fitting results of isothermal adsorption are shown in Fig. 7 and Table 4. The error functions SSE, MSE, and RMSE of the Langmuir model are all smaller than those of the Freundlich model. Additionally, the correlation coefficient of the Langmuir model is 0.994, which is closer to 1. These data strongly indicate that the Langmuir model can more accurately fit the adsorption data of modified ceramsite for lead ions. Using Langmuir model, the calculated maximum adsorption capacity q_{max} was 33.2 mg/g, and the separation factor K_L was 0.33, indicating that the adsorption process can occur spontaneously [43-53].

As shown in Table 5, the adsorption performance of the acid-alkali modified ceramsite prepared in this study has reached the same order of magnitude as common zeolite adsorbents. Considering that the ceramsite are made from solid waste and the modification process is easier to achieve than the preparation process of general zeolites, modified ceramsite has significant advantages in terms of preparation cost and process operability.

Adsorption Mechanism

The better adsorption performance of the modified ceramsite after acid-alkali co-modification mainly stems from two aspects: (1) During the acid treatment process, a composite pore structure is formed on the surface of the ceramsite due to acid corrosion, significantly enhancing the specific surface area, which serves as the fundamental condition for the adsorption capacity of the ceramsite. (2) After the alkaline treatment modification, numerous hydroxyl groups are loaded on the surface of the ceramsite. Hydroxyl groups play an important role in the adsorption of heavy metals. For example, the oxygen atoms on the hydroxyl groups can form coordination bonds with metal cations, thereby binding

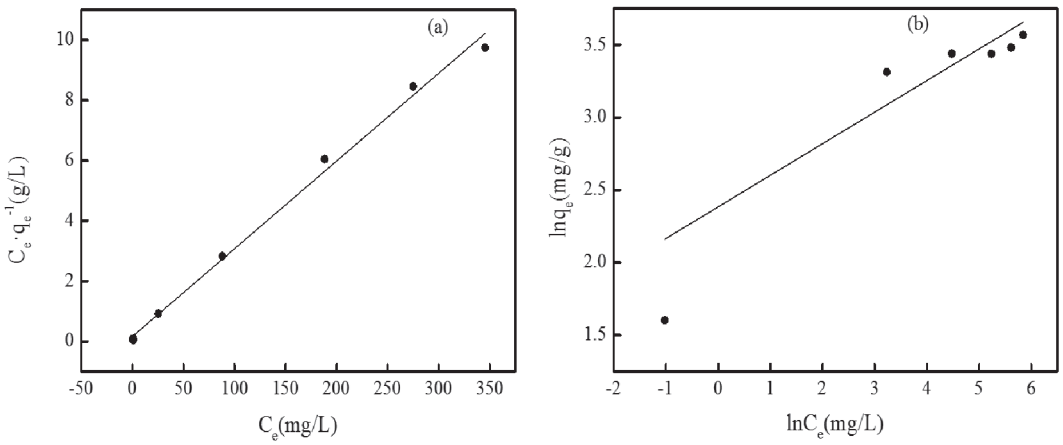

Fig. 7. Isothermal adsorption models and fitting results: a) Langmuir model; b) Freundlich model.

Table 4. Parameters and error functions for two adsorption isotherm models.

	Parameters	SSE	MSE	RMSE	R^2
Langmuir	q_{max} = 33.200, K_L = 0.330	1.163	0.194	0.44	0.995
Freundlich	n = 4.597	162.5	27.083	5.204	0.738

Table 5. Adsorption capacities of Pb^{2+} by modified ceramsite and various zeolite adsorbents.

Adsorbent	Q_{max} (mg/g)	Raw material	Production costs	References
Clinoptilolite	74.6	Commercial chemicals	High	[54]
Natural zeolite	66.0	Natural mineral	Medium	[55]
Na-zeolite	66.9	Commercial chemicals	High	[56]
Modified ceramsite	33.2	Solid waste	Low	This study

the cations to the surface of the ceramsite. Additionally, the modified ceramsite have an isoelectric point pH value is 5.6, which means that under neutral conditions, the negatively charged surface of the modified ceramsite can adsorb cations through electrostatic interaction [57-62].

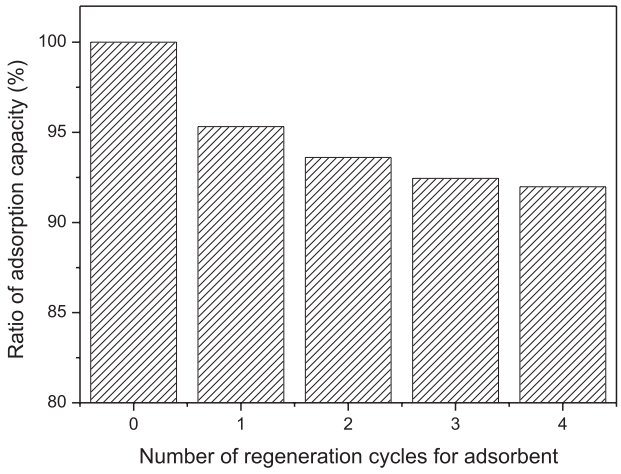

Fig. 8. Regeneration capacity of the modified ceramsite.

Regeneration Capacity

The adsorption capacity of the regenerated adsorbent is shown in Fig. 8. Even after undergoing 4 regeneration cycles, the adsorption capacity of the regenerated ceramsite remained at a high level, with over 90% of the original adsorption capacity still maintained. The regeneration mechanism of the adsorbent is as follows: the alkaline treatment during the regeneration process reloads hydroxyl groups onto the surface of the ceramsite. Hydroxyl groups play a very important role for the adsorption of lead ions by the modified ceramsite, as described in section 3.6. Therefore, the regenerated ceramsite still possess a high adsorption capacity for lead ions.

Conclusions

The present study proposed a low-cost and convenient modification method for ceramsite using acid-alkali treatment, and the modified ceramsite could be used as a adsorbent for Pb^{2+}. The main conclusions are as follows:

(1) Acid treatment can significantly increase the specific surface area of ceramsite through etching

reaction. During the Acid treatment process, some phases in the ceramsite reacted with the acid, resulting in a composite pore structure on the surface of the ceramsite under etching, leading to a significant increase in the specific surface area.

(2) Alkali modification can load hydroxyl groups onto the surface of the ceramsite, significantly improving the heavy metal adsorption capacity. Hydroxyl groups can adsorb lead ions through coordination bonds and electrostatic interactions. The Pseudo-second-order kinetic mode and Langmuir isotherm model can better fit the adsorption data, and the calculated saturated adsorption capacity can reach 33.2 mg/g.

(3) Although the adsorption performance of modified ceramic particles is slightly lower than that of natural zeolite, it is important to consider that they are prepared using solid waste materials under mild conditions. Therefore, modified ceramic particles have significant advantages in terms of raw material sources and production costs.

Acknowledgments

This research was funded by Inner Mongolia Natural Science Foundation (2021MS05054) and program for innovative research team in Universities of Inner Mongolia Autonomous Region (NMGIRT2321). We are also grateful to the anonymous reviewers and all the editors in the process of revision.

Conflict of Interest

The authors declare no conflict of interest.

References

1. GUO X.L., YAO Y.D., YIN G.F., KANG Y.Q., LUO Y., ZHUO L. Preparation of decolorizing ceramsites for printing and dyeing wastewater with acid and base treated clay. Applied Clay Science, **40** (1–4), 20, **2008**.
2. XU G. R., ZOU J.L., LI G.B. Ceramsite made with water and wastewater sludge and its characteristics affected by SiO_2 and Al_2O_3. Environmental Science Technology, **42** (19), 7417, **2008**.
3. WEI Y.L., KO G.W. Recycling steel wastewater sludges as raw materials for preparing lightweight aggregates. Journal of Cleaner Production, **165**, 905, **2017**.
4. LI T.P., SUN T.T., LI D.X. Preparation, sintering behavior, and expansion performance of ceramsite filter media from dewatered sewage sludge, coal fly ash, and river sediment. Journal of Material Cycles and Waste Management, **20** (1), 71, **2018**.
5. LI P.W., LUO S.H., ZHANG L., WANG Q., HUANG X.D., ZHANG Y.H., DUAN X.H. Study on preparation and performance of iron tailings-based porous ceramsite filter materials for water treatment. Separation and Purification Technology, **276**, 119380, **2021**.
6. SHAO Q., ZHANG Y., LIU Z., LONG L.Z., LIU Z.Z., CHEN Y.Q., HUANG L.Z. Phosphorus and nitrogen recovery from wastewater by ceramsite: Adsorption mechanism, plant cultivation and sustainability analysis. Science of the Total Environment, **805**, 150288, **2022**.
7. WANG C., ZHANG F.-S. Zeolite loaded ceramsite developed from construction and demolition waste. Materials Letters, **93**, 380, **2013**.
8. ZHANG L., ZHANG S., LI R. Synthesis of hierarchically porous Na-P zeotype composites for ammonium removal. Environmental Engineering Science, **36** (9), 1089, **2019**.
9. JIA J., HU L., ZHENG J., ZHAI Y., YAO P., ZHAO S., ZHANG, D. Environmental toxicity analysis and reduction of ceramsite synthesis from industrial coal gasification coarse cinder waste. Polish Journal of Environmental Studies, **26** (1), 147, **2017**.
10. CHEN Y., XU W., WANG N., AN S., PENG J., PENG J., SONG X. Synthesis of hierarchical porous ceramsites loaded with GIS-P1 zeolite crystals for removal of ammonia nitrogen from aqueous solution. Journal of Environmental Chemical Engineering, **11** (3), 110221, **2023**.
11. NIU J.R., DING P.J., JIA X.X., HU G.Z., LI Z.X. Study of the properties and mechanism of deep reduction and efficient adsorption of Cr (VI) by low-cost Fe_3O_4-modified ceramsite. Science of the Total Environment, **688**, 994, **2019**.
12. JIANG C., JIA L.Y., ZHANG B., HE Y.L., KIRUMBA G. Comparison of quartz sand, anthracite, shale and biological ceramsite for adsorptive removal of phosphorus from aqueous solution. Journal of Environmental Sciences, **26** (2), 466, **2014**.
13. JING Q.X., WANG Y.Y., CHAI L.Y., TANG C.J., HUANG X.D., GUO H., YOU W. Adsorption of copper ions on porous ceramsite prepared by diatomite and tungsten residue. Transactions of Nonferrous Metals Society of China, **28** (5), 1053, **2018**.
14. WANG J.L., ZHAO Y.L., ZHANG P.P., YANG L.Q., XU H.A., XI G.P. Adsorption characteristics of a novel ceramsite for heavy metal removal from stormwater runoff. Chinese Journal of Chemical Engineering, **26** (1), 96, **2018**.
15. WANG Y.T., GONG S.Y., LI Y.Z., LI Z., FU J. Adsorptive removal of tetracycline by sustainable ceramsite substrate from bentonite/red mud/pine sawdust. Scientific Reports, **10** (1), **2020**.
16. CHEN W., ZHAO H., XUE Y., CHANG X. Adsorption Effect and Adsorption Mechanism of High Content Zeolite Ceramsite on Asphalt VOCs. Materials, **15** (17), 6100, **2022**.
17. LU M., WANG R., XUE Y.J., REN L., CHEN S., LIU J.X., LI J.P. Eco-friendly ceramsite from dredged sediment/biomass for Pb (II) removal: Process optimization and adsorption mechanistic insights. Journal of Environmental Chemical Engineering, **10** (6), **2022**.
18. WANG C., CHEN X. Preparation and characterization of granular zeolite material from construction and demolition waste for lead removal. Desalination and Water Treatment, **72**, 354, **2017**.
19. ZHANG L., ZHANG L., DONG X., ZHANG S., ZHAO Y., CEN Q., ZHANG K. The effect and mechanism of Si/Al ratio on microstructure of zeolite modified ceramsite derived from industrial wastes. Microporous and Mesoporous Materials, **311**, 110667, **2021**.
20. CHEN Y., WANG N., AN S., CAI C., PENG J., XIE M., SONG X. Synthesis of novel hierarchical porous

zeolitization ceramsite from industrial waste as efficient adsorbent for separation of ammonia nitrogen. Separation and Purification Technology, **297**, 121418, **2022**.
21. DARMOKOESOEMO H., MAGDHALENA P.T., KUSUMA H. Telescope snail (*Telescopium* sp) and Mangrove crab (*Scylla* sp) as adsorbent for the removal of Pb^{2+} from aqueous solutions. Rasayan J Chem, **9** (4), 680, **2016**.
22. DARMOKOESOEMO H., SETIANINGSIH F., PUTRANTO T. Horn snail (*Telescopium* sp) and mud crab (Scylla sp) shells powder as low cost adsorbents for removal of Cu^{2+} from synthetic wastewater. Rasayan J Chem, **9** (4), 550, **2016**.
23. KHERA R.A., IQBAL M., AHMAD A. Kinetics and equilibrium studies of copper, zinc, and nickel ions adsorptive removal on to Archontophoenix alexandrae: conditions optimization by RSM. Desalination and Water Treatment, **201**, 289, **2020**.
24. KUNCORO E.P., ISNADINA D.R.M., DARMOKOESOEMO H. Characterization, kinetic, and isotherm data for adsorption of Pb^{2+} from aqueous solution by adsorbent from mixture of bagasse-bentonite. Data in brief, **16**, 622, **2018**.
25. KUNCORO E.P., SOEDARTI, PUTRANTO T.W.C. Characterization of a mixture of algae waste-bentonite used as adsorbent for the removal of Pb^{2+} from aqueous solution. Data in brief, **16**, 908, **2018**.
26. NAAT J.N., NEOLAKA Y.A., LAPAILAKA T. Adsorption of Cu (II) and Pb (II) using silica@ mercapto (hs@m) hybrid adsorbent synthesized from silica of Takari sand: optimization of parameters and kinetics. Rasayan J Chem, **14** (1), 550, **2021**.
27. NEOLAKA Y.A., LAWA Y., NAAT J. Adsorption of methyl red from aqueous solution using Bali cow bones (Bos javanicus domesticus) hydrochar powder. Results in Engineering, 17, 100824, **2023**.
28. CASEY W.H., WESTRICH H.R., ARNOLD G.W. Surface chemistry of labradorite feldspar reacted with aqueous solutions at pH = 2, 3, and 12. Geochimica et Cosmochimica Acta, **52** (12), 2795, **1988**.
29. CASEY W.H., WESTRICH H.R., MASSIS T., BANFIELD J.F., ARNOLD G.W. The surface of labradorite feldspar after acid hydrolysis. Chemical Geology, **78** (3–4), 205, **1989**.
30. MURPHY W.M., HELGESON H.C. Thermodynamic and kinetic constraints on reaction rates among minerals and aqueous solutions. III. Activated complexes and the pH-dependence of the rates of feldspar, pyroxene, wollastonite, and olivine hydrolysis. Geochimica et Cosmochimica Acta, **51** (12), 3137, **1987**.
31. OELKERS E.H., SCHOTT J. An experimental study of enstatite dissolution rates as a function of pH, temperature, and aqueous Mg and Si concentration, and the mechanism of pyroxene/pyroxenoid dissolution. Geochimica et Cosmochimica Acta, **65** (8), 1219, **2001**.

AIGBE U.O., UKHUREBOR K.E., ONYANCHA R.B., OSIBOTE O.A., DARMOKOESOEMO H., KUSUMA H.S. Fly ash-based adsorbent for adsorption of heavy metals and dyes from aqueous solution: a review. Journal of Materials Research and Technology, **14**, 2751, **2021**.

32. BUDIANA I.G.M.N., JASMAN J., NEOLAKA Y.A.B., RIWU A.A.P., ELMSELLEM H., DARMOKOESOEMO H., KUSUMA H.S. Synthesis, characterization and application of cinnamoyl C-phenylcalix [4] resorcinarene (CCPCR) for removal of Cr (III) ion from the aquatic environment. Journal of Molecular Liquids, **324**, 114776, **2021**.
33. MAHRENI M., RAMADHAN R.R., PRAMADHANA M.F., PERMATASARI A.P., KURNIAWATI D., KUSUMA H.S. Synthesis of metal organic framework (MOF) based Ca-Alginate for adsorption of malachite green dye. Polymer Bulletin, **79** (12), 11301, **2022**.
34. NAAT J.N., NEOLAKA Y.A.B., LAPAILAKA T., TJ R.T., SABARUDIN A., DARMOKOESOEMO H., KUSUMA H.S. Adsorption of Cu (II) and Pb (II) using silica@ mercapto (hs@ m) hybrid adsorbent synthesized from silica of Takari sand: optimization of parameters and kinetics. Rasayan J Chem, **14** (1), 550. **2021**.
35. NEOLAKA Y.A.B., LAWA Y., NAAT J., LALANG A.C., WIDYANINGRUM B.A., NGASU G.F., KUSUMA H.S. Adsorption of methyl red from aqueous solution using Bali cow bones (Bos javanicus domesticus) hydrochar powder. Results in Engineering, **17**, 100824, **2023**
36. NEOLAKA Y.A.B., LAWA Y., NAAT J., RIWU A.A.P., DARMOKOESOEMO H., WIDYANINGRUM B.A., KUSUMA H.S. Indonesian Kesambi wood (Schleichera oleosa) activated with pyrolysis and H_2SO_4 combination methods to produce mesoporous activated carbon for Pb (II) adsorption from aqueous solution. Environmental Technology & Innovation, **24**, 101997, **2021**.
37. NEOLAKA Y.A.B., LAWA Y., NAAT J., RIWU A.A.P., LINDU Y.E., DARMOKOESOEMO H., KUSUMA H.S. Evaluation of magnetic material IIP@ GO-Fe_3O_4 based on Kesambi wood (Schleichera oleosa) as a potential adsorbent for the removal of Cr (VI) from aqueous solutions. Reactive and Functional Polymers, **166**, 105000. **2021**.
38. NEOLAKA Y.A.B., LAWA Y., NAAT J., RIWU A.A.P., MANGO A.W., DARMOKOESOEMO H., KUSUMA H.S. Efficiency of activated natural zeolite-based magnetic composite (ANZ-Fe_3O_4) as a novel adsorbent for removal of Cr (VI) from wastewater. Journal of Materials Research and Technology, **18**, 2896, **2022**.
39. NEOLAKA Y.A.B., LAWA Y., NAAT J.N., RIWU A.A.P., IQBAL M., DARMOKOESOEMO H., KUSUMA H.S. The adsorption of Cr (VI) from water samples using graphene oxide-magnetic (GO-Fe_3O_4) synthesized from natural cellulose-based graphite (kusambi wood or Schleichera oleosa): Study of kinetics, isotherms and thermodynamics. Journal of Materials Research and Technology, **9** (3), 6544, **2020**.
40. NEOLAKA Y.A.B., LAWA Y., NAAT J.N., RIWU A.A.P., DARMOKOESOEMO H., SUPRIYANTO G., KUSUMA H.S. A Cr (VI)-imprinted-poly (4-VP-co-EGDMA) sorbent prepared using precipitation polymerization and its application for selective adsorptive removal and solid phase extraction of Cr (VI) ions from electroplating industrial wastewater. Reactive and Functional Polymers, **147**, 104451, **2020**.
41. NEOLAKA Y.A.B., SUPRIYANTO G., KUSUMA H.S. Adsorption performance of Cr (VI)-imprinted poly (4-VP-co-MMA) supported on activated Indonesia (Ende-Flores) natural zeolite structure for Cr (VI) removal from aqueous solution. Journal of Environmental Chemical Engineering, **6** (2), 3436, **2018**.
42. AIGBE U.O., UKHUREBOR K.E., ONYANCHA R.B. Fly ash-based adsorbent for adsorption of heavy metals and dyes from aqueous solution: a review. Journal of Materials Research and Technology, **14**, 2751, **2021**.
43. BUDIANA I.G.M.N., JASMAN J., NEOLAKA Y.A. Synthesis, characterization and application of cinnamoyl

C-phenylcalix [4] resorcinarene (CCPCR) for removal of Cr (III) ion from the aquatic environment. Journal of Molecular Liquids, **324**, 114776, **2021**.
44. MAHRENI M., RAMADHAN R.R., PRAMADHANA M.F. Synthesis of metal organic framework (MOF) based Ca-Alginate for adsorption of malachite green dye. Polymer Bulletin, **79** (12), 11301, **2022**.
45. NAAT J.N., NEOLAKA Y.A., LAPAILAKA T. Adsorption of Cu (II) and Pb (II) using silica@ mercapto (hs@ m) hybrid adsorbent synthesized from silica of Takari sand: optimization of parameters and kinetics. Rasayan J Chem, **14** (1), 550, **2021**.
46. NEOLAKA Y.A., LAWA Y., NAAT J. Indonesian Kesambi wood (Schleichera oleosa) activated with pyrolysis and H2SO4 combination methods to produce mesoporous activated carbon for Pb (II) adsorption from aqueous solution. Environmental Technology & Innovation, **24**, 101997, **2021**.
47. NEOLAKA Y.A., LAWA Y., NAAT J. Evaluation of magnetic material IIP@ GO-Fe_3O4 based on Kesambi wood (Schleichera oleosa) as a potential adsorbent for the removal of Cr (VI) from aqueous solutions. Reactive and Functional Polymers, **166**, 105000, **2021**.
48. NEOLAKA Y.A., LAWA Y., NAAT J. Efficiency of activated natural zeolite-based magnetic composite (ANZ-Fe_3O_4) as a novel adsorbent for removal of Cr (VI) from wastewater. Journal of Materials Research and Technology, **18**, 2896, **2022**.
49. NEOLAKA Y.A., LAWA Y., NAAT J.N. The adsorption of Cr (VI) from water samples using graphene oxide-magnetic (GO-Fe_3O_4) synthesized from natural cellulose-based graphite (kusambi wood or Schleichera oleosa): Study of kinetics, isotherms and thermodynamics. Journal of Materials Research and Technology, **9** (3), 6544, **2020**.
50. NEOLAKA Y.A., LAWA Y., NAAT J.N. A Cr (VI)-imprinted-poly (4-VP-co-EGDMA) sorbent prepared using precipitation polymerization and its application for selective adsorptive removal and solid phase extraction of Cr (VI) ions from electroplating industrial wastewater. Reactive and Functional Polymers, **147**, 104451, **2020**.
51. NEOLAKA Y.A., SUPRIYANTO G., KUSUMA H.S. Adsorption performance of Cr (VI)-imprinted poly (4-VP-co-MMA) supported on activated Indonesia (Ende-Flores) natural zeolite structure for Cr (VI) removal from aqueous solution. Journal of Environmental Chemical Engineering, **6** (2), 3436, **2018**.
52. NEOLAKA Y.A., LAWA Y., NAAT J. Adsorption of methyl red from aqueous solution using Bali cow bones (Bos javanicus domesticus) hydrochar powder. Results in Engineering, **17**, 100824, **2023**.
53. SHIRZADI H., NEZAMZADEH-EJHIEH A. An efficient modified zeolite for simultaneous removal of Pb (II) and Hg (II) from aqueous solution. Journal of Molecular Liquids, **230**, 221, **2017**.
54. KRAGOVIĆ M., DAKOVIĆ A., MARKOVIĆ M., KRSTIĆ J., GATTA G.D., ROTIROTI N. Characterization of lead sorption by the natural and Fe (III)-modified zeolite. Applied Surface Science, **283**, 764, **2013**.
55. YUAN M., XIE T., YAN G., CHEN Q., WANG L. Effective removal of Pb^{2+} from aqueous solutions by magnetically modified zeolite. Powder Technology, **332**, 234, **2018**.
56. KUNCORO E.P., SOEDARTI T., PUTRANTO T.W.C. Characterization of a mixture of algae waste-bentonite used as adsorbent for the removal of Pb^{2+} from aqueous solution. Data in brief, **16**, 908. **2018**.
57. KUNCORO E.P., ISNADINA D.RM., DARMOKOESOEMO H. Characterization, kinetic, and isotherm data for adsorption of Pb^{2+} from aqueous solution by adsorbent from mixture of bagasse-bentonite. Data in brief, **16**, 622, **2018**.
58. NEOLAKA Y.A., LAWA Y., NAAT J. Evaluation of magnetic material IIP@ GO-Fe_3O_4 based on Kesambi wood (Schleichera oleosa) as a potential adsorbent for the removal of Cr (VI) from aqueous solutions. Reactive and Functional Polymers, **166**, 105000, **2021**.
59. NEOLAKA Y.A., LAWA Y., NAAT J. Efficiency of activated natural zeolite-based magnetic composite (ANZ-Fe_3O_4) as a novel adsorbent for removal of Cr (VI) from wastewater. Journal of Materials Research and Technology, **18**, 2896, **2022**.
60. NEOLAKA Y.A., SUPRIYANTO G., DARMOKOESOEMO H. Characterization, isotherm, and thermodynamic data for selective adsorption of Cr (VI) from aqueous solution by Indonesia (Ende-Flores) natural zeolite Cr (VI)-imprinted-poly (4-VP-co-EGDMA)-ANZ (IIP-ANZ). Data in brief, **17**, 1020, **2018**.
61. NEOLAKA Y.A., SUPRIYANTO G., DARMOKOESOEMO H. Characterization, kinetic, and isotherm data for Cr (VI) removal from aqueous solution by Cr (VI)-imprinted poly (4-VP-co-MMA) supported on activated Indonesia (Ende-Flores) natural zeolite structure. Data in brief, **17**, 969, **2018**.